Effect of Al on the sharpness of the $MgSiO_3$ perovskite to post-perovskite phase transition

S. Akber-Knutson,[1] G. Steinle-Neumann,[2] and P. D. Asimow[1]

Received 8 April 2005; revised 8 June 2005; accepted 13 June 2005; published 19 July 2005.

[1] By means of static ab-initio computations we investigate the influence of Al on the recently discovered perovskite to post-perovskite phase transition in $MgSiO_3$. We examine three substitution mechanisms for Al in the two structures: MgSi → AlAl; SiSiO → AlAl□; and Si → AlH. The substitutions introducing oxygen vacancies (highly unfavorable, energetically) and water (favorable) both lower the 0 Kelvin transition pressure, whereas charge coupled substitution increases it relative to 105 GPa for pure $MgSiO_3$. From the transition pressures for 0, 6.25, and 100 mol% charge coupled Al_2O_3 incorporation and simple solution theories, we estimate the phase diagram of Al-bearing $MgSiO_3$ at low Al concentrations. Assuming the Clapeyron slope is independent of Al concentration, we find the perovskite-to-post-perovskite transition region to span 127–140 GPa, at 6.25 mol% Al_2O_3. When the upper pressure limit is bounded by the core-mantle boundary, the phase coexistence region has width 150 km. **Citation:** Akber-Knutson, S., G. Steinle-Neumann, and P. D. Asimow (2005), Effect of Al on the sharpness of the $MgSiO_3$ perovskite to post-perovskite phase transition, *Geophys. Res. Lett.*, *32*, L14303, doi:10.1029/2005GL023192.

1. Introduction

[2] At the base of the Earth's mantle lies a distinct layer a few hundred kilometers thick. This layer, known as D″, serves as a thermal and chemical boundary layer between silicate mantle rock and molten iron alloy outer core [*Lay et al.*, 2004]. Its distinguishing features include a sharp discontinuity (of about 1%) in density and shear wave velocity [*Sidorin et al.*, 1998] in some places, and a low velocity layer in other places [*Garnero et al.*, 1993]. The large lateral seismic heterogeneity and observed negative correlation between shear and bulk sound speed cannot be explained by thermal variations alone [*Su and Dziewonski*, 1997; *Vasco and Johnson*, 1998; *Masters et al.*, 2000]. Additionally, seismic observations indicate shear wave splitting in the D″ [*Garnero and Lay*, 1997]. These features potentially provide valuable constraints on its nature and may be attributed to core-mantle reactions [*Knittle and Jeanloz*, 1989, 1991], subduction debris [*Van der Voo et al.*, 1999], a phase change in mantle minerals, or a combination of the above.

[3] The discovery of $MgSiO_3$ post-perovskite, stable at lowermost mantle conditions, provides one of the possibilities mentioned, and has led to numerous efforts to integrate this phase into the current view of the D″ layer. According to experimental [*Murakami et al.*, 2004; *Shim et al.*, 2004; *Oganov and Ono*, 2004] and computational work [*Iitaka et al.*, 2004; *Oganov and Ono*, 2004; *Tsuchiya et al.*, 2004], the structural transformation from $MgSiO_3$ perovskite to post-perovskite occurs along a univariant line of positive Clapeyron slope passing through 125 GPa at 2100 K and up to 145 GPa at 2600 K, coinciding with D″ conditions: 127–136 GPa, 2800–4000 K. The computed jumps in density and acoustic velocities [*Oganov and Ono*, 2004] are consistent with seismic observations [*Sidorin et al.*, 1998], and the ab initio molecular dynamics simulations of [*Stackhouse et al.*, 2005] determined that there is enough anisotropy in post-perovskite to explain the observed shear wave splitting.

[4] However, work has focused largely on pure $MgSiO_3$, for which the univariant transition is sharp; realistic mantle compositions include Al and Fe. The width of the transition is entirely a function of the partitioning of such elements between the two phases and the resulting phase equilibria. Furthermore, the effects of these elements on the transition depth and Clapeyron slope have not been tested. Therefore, further investigation of post-perovskite as a viable source of the observed D″ characteristics is warranted.

[5] Here we conduct static, 0 Kelvin first-principles calculations to explore the effects of Al_2O_3 on the perovskite to post-perovskite transition. We find that at pyrolitic abundances (6.25 mol% Al_2O_3 in $MgSiO_3$), Al increases the transition pressure by 7 GPa, or transition depth by ∼115–120 km. We use the transition pressures at three Al_2O_3 concentrations (0, 6.25, and 100 mol%), together with reasonable choices of simple solution models, to determine the phase diagram of $MgSiO_3$ as a function of Al concentration. Thus we constrain the coexistence depths of the two phases in the presence of Al_2O_3. We find a smooth transition over ∼150 km, extending to pressures just below CMB pressures (127–140 GPa). This suggests that, in the presence of Al, the perovskite to post-perovskite phase transition may not explain the sharp discontinuity at the top of the D″ layer; however, it is consistent with a wide region of negative correlation between bulk and shear wave velocities.

2. Computational Technique

[6] Internal energies are computed from first-principles calculations based on density functional theory, using fixed-volume cell optimizations with respect to cell shape, atomic positions, and electronic wave functions. We use the Vienna Ab Initio Simulations Program (VASP) [*Kresse and Furthmüller*, 1996a, 1996b]. Electronic exchange and

[1]Division of Geological and Planetary Sciences, California Institute of Technology, Pasadena, California, USA.
[2]Bayerisches Geoinstitut, University of Bayreuth, Bayreuth, Germany.

0094-8276/05/2005GL023192$05.00

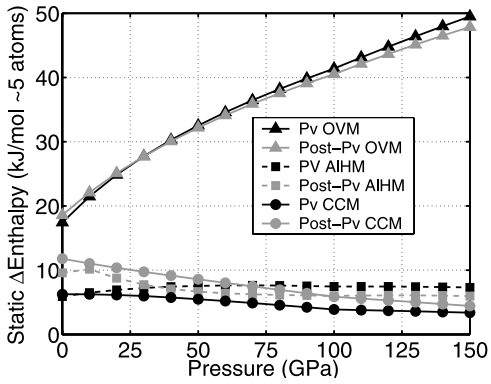

Figure 1. Enthalpies of solution for various mechanisms of Al_2O_3 incorporation into $MgSiO_3$ perovskite and post-perovskite structures.

correlation are approximated within the Generalized Gradient Approximation (GGA) [*Perdew*, 1991]. Pseudo-wave functions describe the core electrons [*Vanderbilt*, 1990; *Kresse and Hafner*, 1994] of Mg, Al, Si, H, and O, with core radii (in Bohr) of 2.000, 1.820, 1.800, 1.250, and 1.550. Plane waves of kinetic energy up to 1000 eV are included, and the electronic *k*-grids are described by Monkhorst-Pack grids [*Monkhorst and Pack*, 1976] of 2^3 for 80-atom cells, 4^3 for 20-atom cells, 8^3 for MgO periclase, and 12^3 for Ice X. These cut-offs and grids guarantee total energy convergence to within 1 meV per atom.

[7] We test the pseudopotentials by computing equations of state for relevant $MgSiO_3$ and Al_2O_3 polymorphs and find good agreement with previously published ab-initio results[1]. Equations of state are obtained from fitting internal energy versus volume to the third-order Birch-Murnaghan equation of state. From this we get static Helmholtz free energy and volume as functions of pressure, and may calculate the static Gibbs free energy and relative stabilities:

$$G_{static}(P) = F_{static}(V(P)) + PV_{static}(P) \quad (1)$$

We consider three Al incorporation mechanisms into $MgSiO_3$: MgSi → AlAl (charge coupled mechanism: CCM), SiSiO → AlAl□ (oxygen vacancy forming substitution: OVM), and Si → AlH (hydrous Al substitution: AlHM). In each case, the cell contains 80 atoms. For CCM, Al_2O_3 concentrations include 6.25 and 100 mol%, for OVM, 6.25 mol%, and for AlHM, 3.125 mol%. In the first two cases, several choices of Al arrangement are available; we choose ones having the lowest static enthalpies, narrowing our search based on previous work [*Akber-Knutson and Bukowinski*, 2004] for Al-bearing $MgSiO_3$ perovskite and testing several cases for post-perovskite.

[8] Volume ranges for internal energy calculations were chosen to provide good equation of state fits at low pressures and to reach pressures just above 200 GPa. In most cases, this corresponds to a volume range of approximately 105–65% of V_0.

3. Results

[9] Enthalpies of solution for Al incorporation into perovskite and post-perovskite structures indicate that oxygen vacancy substitution is highly unfavorable in both phases (Figure 1). If water is available, the substitution of AlH for Si has a small, positive enthalpy of mixing, relative to ice X; this is easily overcome at finite temperature by the entropy of mixing, yielding a negative Gibbs free energy of mixing. In the anhydrous case, one need only consider charge coupled substitution. From the CCM enthalpies of solution, it is apparent that at a fixed concentration of 6.25 mol%, Al_2O_3 is more soluble in perovskite than in post-perovskite. Thus one would expect this amount of Al to stabilize perovskite with respect to post-perovskite and increase the transition pressure.

[10] Static enthalpy differences between post-perovskite and perovskite in various substitutions indicate that Al → Si type substitutions stabilize the former, whereas coupled substitutions stabilize the latter (Figure 2). While OVM may be neglected, the effect of even a small amount of AlH in $MgSiO_3$ on decreasing the transition pressure to 99 GPa is notable. On the other hand, CCM, at 6.25 and 100 Al2O_3 mol%, increases the transition pressure to 112 and 113 GPa, respectively. Equations of state are summarized in Table 1. CCM expands the volume and lowers the bulk modulus of perovskite, whereas it decreases the volume and does not much affect the bulk modulus of post-perovskite.

[11] Calculations are carried out with equal Al concentrations in the two phases; an equilibrium pressure determined by this means is "pseudo-univariant." However, the end-member equilibria in pure $MgSiO_3$ and Al_2O_3 and one pair of such calculations for Al-bearing perovskite and post-perovskite at equal concentration are sufficient to determine the divariant phase loop of Al-bearing $MgSiO_3$, if a reasonable assumption about the form of solution model is made. We show the results of two such models for both phases: Henry's Law for dilute Al_2O_3 concentrations, and symmetric regular solutions for the whole binary. In both cases we focus on the CCM for Al incorporation.

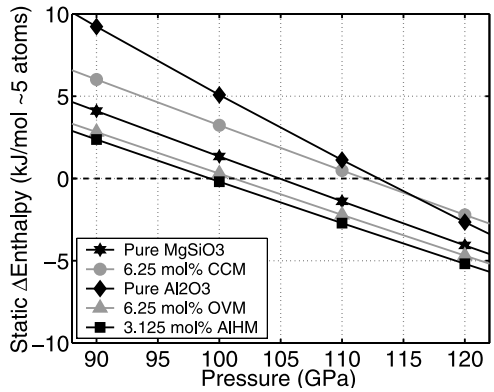

Figure 2. Enthalpy differences between post-perovskite and perovskite as functions of pressure for various Al_2O_3 substitution mechanisms. The zero-crossings mark transition pressures.

[1]Auxiliary material is available at ftp://ftp.agu.org/apend/gl/2005GL023192.

Table 1. Equations of State for Al-Bearing $MgSiO_3$ Perovskite and Post-Perovskite[a]

Substitution	Al_2O_3, mol%	V_0 (Å^3)	K_0, GPa	K'
		Perovskite		
None	0	41.75	235	3.84
CCM	6.25	41.86	232	3.86
CCM	100	42.83	205	4.03
OVM	6.25	42.36	214	3.96
AlHM	3.125	42.20	228	3.85
		Post-Perovskite		
None	0	41.83	204	4.18
CCM	6.25	41.79	207	4.13
CCM	100	41.78	201	4.29
OVM	6.25	42.33	194	4.15
AlHM	3.125	41.64	228	3.86

[a]All values have been normalized for approximately 5-atom unit cells; for 6.25 mol% Al_2O_3 in OVM this corresponds to 79/16 atoms, and in AlHM to 81/16 atoms.

[12] To derive both constructions, we begin with the end-member equilibrium at the transition pressure, P_0.

$$\mu^{o\,Pv}_{MgSiO_3}(P_0) = \mu^{o\,Post-Pv}_{MgSiO_3}(P_0) \tag{2}$$

where μ^{ϕ}_{c} is the chemical potential of component c in phase ϕ. At an arbitrary pressure P where the volume change is not too large, relative to that at P_0, equation (2) can be re-written by relating volume to the Gibbs free energy and pressure ($V = \partial G/\partial P$).

$$\mu^{o\,\phi}_{MgSiO_3}(P) = \mu^{o\,\phi}_{MgSiO_3}(P_0) + V^{\phi}_{MgSiO_3}(P - P_0) \tag{3}$$

where ϕ is either perovskite or post-perovskite. If the pseudounivariant calculation at Al_2O_3 fraction X_1 yields the transition pressure P_1, then

$$\bar{G}^{Pv}_{(MgSi)_{1-X_1}Al_{X_1}O_3}(P_1) = \bar{G}^{Post-Pv}_{(MgSi)_{1-X_1}Al_{X_1}O_3}(P_1) \tag{4}$$

If we write expressions for the chemical potential of each component for the solutions models of interest, then the Gibbs free energy is obtained by summation of chemical potentials over mole fractions, and equation (4) can be solved for an unknown parameter in the solution models.

[13] In the first model, for low Al_2O_3 concentrations, one may use Raoult's Law for $MgSiO_3$, at temperature T,

$$\mu^{\phi}_{MgSiO_3} = \mu^{o\,\phi}_{MgSiO_3} + RT\ln\left(1 - X^{\phi}_{Al_2O_3}\right) \tag{5}$$

where R is the universal gas constant, and Henry's Law for Al_2O_3,

$$\mu^{\phi}_{Al_2O_3} = \mu^{o\,\phi}_{Al_2O_3} + RT\ln h^{\phi}_{Al_2O_3}X^{\phi}_{Al_2O_3} \tag{6}$$

$$= \mu^{\dagger\,\phi}_{Al_2O_3} + RT\ln X^{\phi}_{Al_2O_3} \tag{7}$$

where Henry's constant is absorbed into the converted standard state. The present work with 0 and 6.25 mol% Al_2O_3 in $MgSiO_3$ yields a difference between converted standard states for Post-Pv and Pv of $\Delta\mu^{\dagger} = 29$ kJ/mol.

[14] For the regular solution model, we instead use:

$$\mu^{\phi}_{MgSiO_3} = \mu^{o\,\phi}_{MgSiO_3} + RT\ln\left(1 - X^{\phi}_{Al_2O_3}\right) + W^{\phi}\left(X^{\phi}_{Al_2O_3}\right)^2 \tag{8}$$

$$\mu^{\phi}_{Al_2O_3} = \mu^{o\,\phi}_{Al_2O_3} + RT\ln X^{\phi}_{Al_2O_3} + W^{\phi}\left(1 - X^{\phi}_{Al_2O_3}\right)^2 \tag{9}$$

where W^{ϕ} is an interaction parameter representing deviation from ideality. From the excess enthalpies derived in this work, $W^{Pv} = 40$ kJ/mol and $W^{Post\text{-}Pv} = 69$ kJ/mol.

[15] At any condition where Pv and Post-Pv coexist,

$$\mu^{Pv}_{Al_2O_3} = \mu^{Post-Pv}_{Al_2O_3} \tag{10}$$

$$\mu^{Pv}_{MgSiO_3} = \mu^{Post-Pv}_{MgSiO_3} \tag{11}$$

From the pure end-member transition pressures and phase volumes, and from the pseudo-univariant transition pressure (P_1) at Al_2O_3 concentration (X_1), we obtain the phase diagrams in Figure 3, using Henry's Law and the regular solution model[1] at $T = 2500$ K. Note that our 100% Al_2O_3 calculation does not lie at the position extrapolated using Henry's law from the 0 and 6.25% calculations; we therefore warn that there must be a deviation from Henry's law at some Al_2O_3 concentration. The regular solution model fits all three concentrations and predicts this deviation, including a miscibility gap in Post-Pv at Al_2O_3 concentrations and pressures higher than those relevant to the lower mantle. Possible complexities, which can be investigated with calculations at more concentrations, include narrowing of the phase loop around basaltic Al_2O_3 concentrations.

4. Discussion and Conclusion

[16] It is apparent that with even a small amount of Al_2O_3, $MgSiO_3$ perovskite and post-perovskite coexist over a large range in pressure (~109–122 GPa at 0 K and 6.25% Al_2O_3). Assuming that the Clapeyron slope given by

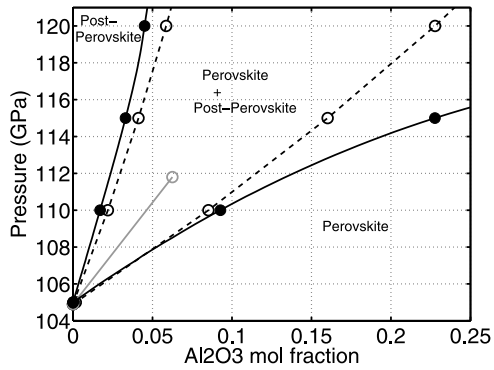

Figure 3. Phase diagram of $MgSiO_3$, for MgSi → AlAl substitution. The dashed curves are derived from Henry's Law, whereas the solid black curves are from regular solution theory. The gray curve corresponds to the pseudo-univariant phase transition. A temperature of 2500 Kelvin was assumed.

[*Tsuchiya et al.*, 2004] for pure $MgSiO_3$ applies to the whole phase loop, the pressure range at 2500 K becomes ~127–140 GPa. If we limit the upper pressure to that of the core-mantle boundary (136 GPa), and use the Preliminary Reference Earth Model [*Dziewonski and Anderson*, 1981] to convert pressure to depth, then the phases coexist over ~2740–2890 km. We find that the post-perovskite phase transition may therefore not be sufficient to explain a seismically sharp discontinuity at the top of the D″ layer. This broad region of phase coexistence is, however, consistent with the seismically observed negative correlations between shear and bulk sound velocity.

[17] There are additional issues to consider regarding the phase transition width. If the Clapeyron slope decreases with increasing Al concentration, then it is possible to recover a relatively sharp transition in the divariant case at high temperature; this remains to be tested. Furthermore, increasing the temperature decreases the width of the phase loop, but increases the transition depth. These trade-offs must be considered. Our calculations do not account for the effects of Fe in any oxidation or spin state. However, it seems unlikely that adding more components and increasing the variance of the coexistence region would narrow the transition, though this should also be tested.

[18] Last, we note that the relative abundances of the coexisting phases vary nonlinearly with pressure, with most of the change occurring at lower pressure. Since we ignore pressures larger than 136 GPa, we need not correct further for this effect. Additionally, the apparent phase transition width, as observed seismically, may differ from the actual, petrologically determined width. For upper mantle transitions, the apparent width can be calculated under the assumption of normal incidence [*Stixrude*, 1997]. This approximation does not apply to the D″, where ray incidence angles range from 70 to 80 degrees. An extension of the treatment to larger ray angles is not straightforward, and a more direct, seismic forward modeling approach would be required to determine whether the phase transition structure predicted for multicomponent mantle compositions would be seismically visible.

[19] **Acknowledgments.** We thank two anonymous reviewers and R. Caracas, E. J. Garnero, D. V. Helmberger, T. Lay, and L. Stixrude for helpful comments. This work is funded by ASCI (U. S. D. O. E. contract W-7405-ENG-48) and the Bayerisches Geoinstitut Visitor Program.

References

Akber-Knutson, S., and M. S. T. Bukowinski (2004), The energetics of aluminum solubility into $MgSiO_3$ perovskite at lower mantle conditions, *Earth Planet. Sci. Lett.*, *220*, 317–330.

Dziewonski, A. M., and D. L. Anderson (1981), Preliminary reference Earth model, *Phys. Earth Planet. Inter.*, *25*, 297–356.

Garnero, E. J., and T. Lay (1997), Lateral variations in lowermost mantle shear wave anisotropy beneath the North Pacific and Alaska, *J. Geophys. Res.*, *102*, 8121–8135.

Garnero, E. J., S. P. Grand, and D. V. Helmberger (1993), Low P-wave velocity at the base of the mantle, *Geophys. Res. Lett.*, *20*, 1843–1846.

Iitaka, T., K. Hirose, K. Kawamura, and M. Murakami (2004), The elasticity of the $MgSiO_3$ post-perovskite phase in the Earth's lowermost mantle, *Nature*, *430*, 442–445.

Knittle, E., and R. Jeanloz (1989), Simulating the core-mantle boundary: An experimental study of high-pressure reactions between silicates and liquid iron, *Geophys. Res. Lett.*, *16*, 609–612.

Knittle, E., and R. Jeanloz (1991), The Earth's core-mantle boundary: Results of experiments at high pressures and temperatures, *Science*, *251*, 1438–1443.

Kresse, G., and J. Furthmüller (1996a), Efficient interative schemes for ab initio total-energy calculations using a plane-wave basis set, *Phys. Rev. B*, *54*, 11,169–11,186.

Kresse, G., and J. Furthmüller (1996b), Efficiency of ab initio total energy calculations for metals and semiconductors using a plane-wave basis set, *Comput. Mater. Sci.*, *6*, 15–50.

Kresse, G., and J. Hafner (1994), Norm-conserving and ultrasoft pseudopotentials for first-row and transition elements, *J. Phys. Condens. Matter*, *6*(40), 8245–8257.

Lay, T., E. J. Garnero, and Q. Williams (2004), Partial melting in a thermo-chemical boundary layer at the base of the mantle, *Phys. Earth Planet. Inter.*, *146*(3-4), 441–467.

Masters, G., G. Laske, H. Bolton, and A. Dziewonski (2000), The relative behavior of shear velocity, bulk sound speed, and compressional velocity in the mantle: Implications for chemical and thermal structure, in *Earth's Deep Interior: Mineral Physics and Tomography from the Atomic to the Global Scale*, *Geophys. Monogr. Ser.*, vol. 117, edited by S.-I. Karato et al., pp. 63–87, AGU, Washington, D. C.

Monkhorst, H. J., and J. D. Pack (1976), Special points for Brillouin-zone integrations, *Phys. Rev. B*, *13*, 5188–5192.

Murakami, M., K. Hirose, K. Kawamura, N. Sata, and Y. Ohishi (2004), Post-perovskite phase transition in $MgSiO_3$, *Science*, *304*, 855–858.

Oganov, A. R., and S. Ono (2004), Theoretical and experimental evidence for a post-perovskite phase of $MgSiO_3$ in Earth's D″ layer, *Nature*, *430*, 445–448.

Perdew, J. P. (1991), Generalized gradient approximations for exchange and correlation: A look backward and forward, *Physica B*, *172*(1-2), 1–6.

Shim, S.-H., T. S. Duffy, R. Jeanloz, and G. Shen (2004), Stability and crystal structure of $MgSiO_3$ perovskite to the core-mantle boundary, *Geophys. Res. Lett.*, *31*, L10603, doi:10.1029/2004GL019639.

Sidorin, I., M. Gurnis, D. V. Helmberger, and X. Ding (1998), Interpreting D″ seismic structure using synthetic waveforms computed from dynamic models, *Earth Planet. Sci. Lett.*, *163*, 31–41.

Stackhouse, S., J. P. Brodholt, J. Wookey, J.-M. Kendall, and G. D. Price (2005), The effect of temperature on the seismic anisotropy of the perovskite and post-perovskite polymorphs of $MgSiO_3$, *Earth Planet. Sci. Lett.*, *230*, 1–10.

Stixrude, L. (1997), Structure and sharpness of phase transitions and mantle discontinuities, *J. Geophys. Res.*, *102*, 14,835–14,852.

Su, W. J., and A. M. Dziewonski (1997), Simultaneous inversion for 3-D variations in shear and bulk velocity in the mantle, *Phys. Earth Planet. Inter.*, *100*, 135–156.

Tsuchiya, T., J. Tsuchiya, K. Umemoto, and R. M. Wentzcovitch (2004), Phase transition in $MgSiO_3$ perovskite in the Earth's lower mantle, *Earth Planet. Sci. Lett.*, *224*, 241–248.

Vanderbilt, D. (1990), Soft self-consistent pseudopotentials in a generalized eigenvalue formalism, *Phys. Rev. B*, *41*, 7892–7895.

Van der Voo, R., W. Spakman, and H. Bijwaard (1999), Mesozoic subducted slabs under Siberia, *Nature*, *397*, 246–249.

Vasco, D. W., and L. R. Johnson (1998), Whole Earth structure estimated from seismic arrival times, *J. Geophys. Res.*, *103*, 2633–2671.

S. Akber-Knutson, Division of Geological and Planetary Sciences, Mail Code 252-21, California Institute of Technology, Pasadena, CA 91125, USA. (sofia@gps.caltech.edu)

P. D. Asimow, Division of Geological and Planetary Sciences, Mail Code 170-25, California Institute of Technology, Pasadena, CA 91125, USA. (asimow@gps.caltech.edu)

G. Steinle-Neumann, Bayerisches Geoinstitut, University of Bayreuth, D-95440 Bayreuth, Germany. (g.steinle-neumann@uni-bayreuth.de)